Photograph-LIDAR Registration Methodology for Rock Discontinuity Measurement

Brittany Morago, Giang Bui, Truc Le, Norbert H. Maerz, and Ye Duan

***Abstract*—Rock detachment events along roadways pose public safety concerns but can be predicted and safely handled using geological measurements of discontinuities. With modern sensing technology, these measurements can be taken on 3D point clouds and 2D optical images that provide a high level of structural accuracy and visual detail. Doing so allows engineers to obtain needed data with relative ease while eliminating the biases and hazards inherent in taking manual measurements. This letter presents an approach for fusing 2D and 3D data in natural and unstructured scenes. This includes a novel method for visualizing imagery obtained with very different sensors to maximize their visual similarity making registration a more tangible task. To show the effectiveness of our registration methodology, we evaluate measurements taken manually and digitally on rock facet and cut discontinuity orientations in Rolla, Missouri. Our method is able to align 2D and 3D data with an accuracy of under 2 cm. The median difference between measurements manually obtained by a geological engineer and those obtained with our proposed software is 3.65 degrees.**

***Index Terms*—Terrestrial LIDAR, Discontinuities, Orientation, Measurement, 2D-3D Registration.**

I. Introduction

IN mountainous and hilly regions, roadways commonly pass alongside tall walls of rocks. This poses many potential obstacles and dangers for drivers, road workers, and engineers who travel through these areas or who are responsible for building and maintaining the road infrastructure [1]. Discontinuities in the rocks oftentimes cause rock mass to break off along existing planar discontinuities that occur either naturally or as a result of engineered rock cutting during the road construction process [2]. By using analytical tools, the arrangement and orientations of single discontinuities or groups of discontinuities can actually be used to study rock stability and predict detachment events [2]. However, obtaining the measurements manually tends to be slow and cumbersome and, in some cases, dangerous because of potentially falling rock [3]. Due to time constraints and safety concerns, they are often only able to be employed in easily accessible locations like the base of a slope [4]. These types of restrictions cans cause sampling biases and inaccuracies [5]. However, modern sensing technologies such as photographs and LIDAR (Light Detection and Ranging) laser scans can be used to capture data more quickly and safely than traditional techniques [6], [7], [8].

This work is supported by awards NSF CMMI #0856420 and #0856206, NSF CC-NIE #1245795, and NSF MRI #1725057.

Measurements on photographs can provide information about trace and discontinuity orientations on rock faces [9]. This can be done by restricting the camera to specific locations around the rock site, having a known configuration between stereo cameras, or by reconstructing the scene from a Structure from Motion (SfM) point cloud [2], [10], [11]. While using exclusively 2D digital photographs is a simple, economical approach, the requirement for computing an SfM point cloud can pose a roadblock as there is not a general solution for creating an accurate reconstruction from every dataset [12]. Overcoming the challenge of using a general SfM algorithm by constricting camera movement can also eliminate flexibility in collecting a full, detailed dataset.

Terrestrial LIDAR scanners can also be utilized to provide highly accurate 3D point clouds of surfaces from which engineers can determine 3D orientations of fractures on irregular surfaces [13], [14], [15], [16], [17]. Planar polygonal models can be generated from LIDAR scans yielding 3D orientations of rock faces [18]. This approach can be complicated by the presence of vegetation or blasting and weathering-induced fractures which need to be identified by sophisticated filters or with the aid of human interaction. Many algorithms using this data semi-automatically extract planar features from the scan, calculate orientations, cluster the orientations, and present them on a stereonet [17], [19].

Despite the abundance of information that can be extracted from 2D or 3D data separately, neither technology, on its own, is sufficient for making measurements on both planar and irregular surfaces. Since it is common for rocks to contain discontinuities on both types of surfaces, we have developed an approach for taking measurements that improves upon existing methods by fusing photographs and LIDAR scans to perform a single analysis using both types of data. We show how we can use data typically available with LIDAR scans to visualize edge and texture properties of 3D scans that can also be easily identified in 2D photographs. By doing so, linear trace measurements that are easily taken on a 2D photograph automatically contain information about 3D facet orientations. Many groups have studied directly registering 2D photographs with 3D LIDAR scans but most are designed for urban data and rely on identifying structural features such as parallel and orthogonal line segments, circles, rectangles, or repetitive pattens that can be matched across dimensions [20], [21], [22], [23]. Since we cannot make the assumption that any of these types of features will be consistently available in natural imagery, we have developed

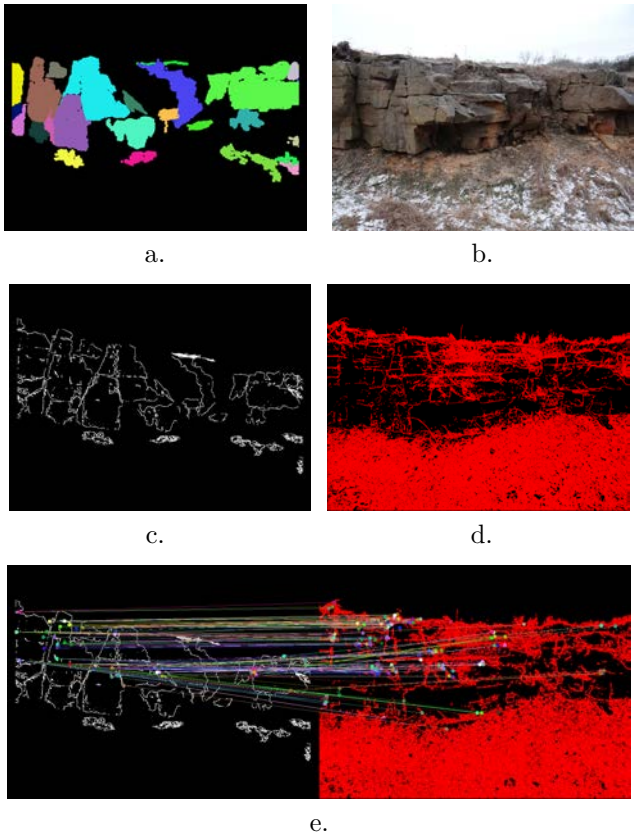

Fig. 1. Matching edge images to 3D wireframe model. *a:* Planar segmentation of 3D scan. *b:* Original photograph. *c:* Wireframe model from same synthetic view as *a*. *d:* Canny Edge image of photograph. *e:* Keypoint matches between edge images.

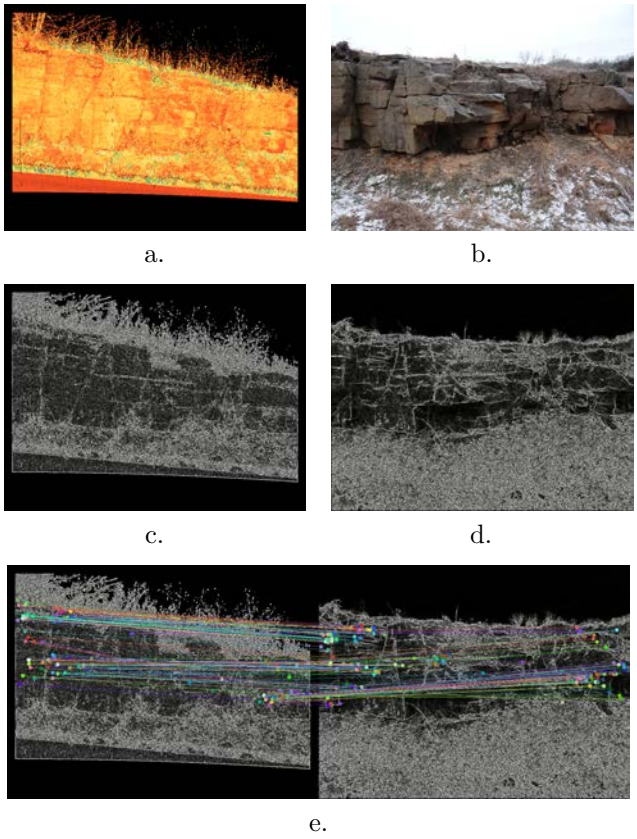

Fig. 2. Matching gradient images to 3D reflectivity images. *a:* 3D scan colored with reflectivity information shown from the perspective of a synthetic camera. *b:* Original photograph. *c:* Gradient magnitude of reflectivity image. *d:* Gradient magnitude of photograph. *e:* Keypoint matches between gradient magnitude images.

a scheme to focus on less constrained environments.

To summarize, our main contributions to this area include:

- A 2D-3D registration method that works on natural, non-urban data. We are not reliant on predictable features such as repetitive structures, circular structures, identifiable vanishing lines, etc.
- A registration method that does not make assumptions about relative camera positions to the scanner or the scene itself. This provides more flexibility in data collection.
- Software to accurately and easily select areas of a 3D point cloud without extensive user training and/or specialized software or equipment. We accomplish this by using both 2D and 3D data. Taking measurements directly on 3D data poses many usability issues[24], [25].

II. Data Acquisition and Pre-Processing

We used Leica C10 HDS and ScanStation II LIDAR scanners to collect 3D scans of the rocky walls alongside roadways in Rolla, MO. Both scanners have a positional accuracy of 6mm, a distance accuracy of 4 mm, and a resolution of less than 1 mm. The vertical rock cuts scanned are within an area of 30x6 m. Throughout our paper, the data obtained with the C10 HDS scanner is

Fig. 3. Views of our 3D registration results on Scan 1 (*a*) and Scan 2 (*b*).

referred to as Scan 1 (S1) and that obtained with the ScanStation II is referred to as Scan 2 (S2).

We create synthetic cameras throughout the scene and use their pose information to visualize a variety of perspectives of each LIDAR scan. Synthetic cameras are placed at regularly spaced intervals and are rotated through different orientations and focused with different focal lengths as described in [26]. We visualize and color the 3D scan using the techniques described in Section III and project this information down onto the 2D synthetic camera planes to create different images of the scan.

During our 2D-3D registration stage, we are primarily interested in the planar, rocky portions of the data. To focus on these areas, we use a RANSAC-based (Random

TABLE I
Feature Repeatability

—	Harris	SIFT	Pseudo Corners
S1 - Wireframe	0.089611	0.609874	0.465327
S2 - Wireframe	0.0785308	0.331122	0.273513
S1 - Reflectivity	0.157935	0.546956	0.368575
S2 - Reflectivity	0.181783	0.373471	0.358221

TABLE II
2D Match Measurements

—	# Matches	# Inliers	Precision	Avg. Error
S1 - Wireframe	38.600	23.600	0.611	1.47209
S2 - Wireframe	57.385	35.615	0.621	1.93076
S1 - Reflectivity	71.800	68.000	0.947	1.83038
S2 - Reflectivity	100.385	75.846	0.756	2.29397
S1 - All	110.4	77.800	0.705	1.90642
S2 - All	154.077	90.385	0.586	2.19393

Sample Consensus) segmentation algorithm similar to the one described in [18] to find 3D planes and segment rock faces from vegetation and the ground plane. The result of this is shown in Figure 1 a.

III. 2D-3D Registration

In order to register an image with the LIDAR range scan, we find a set of correspondences between each photograph and synthetic views. To accomplish this, we visualize two different properties of the LIDAR data that are also captured in photographs.

The first type of information we extract and visualize is a set of 3D edges from which we can create a wireframe model, as seen in Figure 1. Our wireframe model emphasizes the geometrically intrinsic, lighting independent edges contained in a LIDAR scan which are also visible in edge images of photographs. During our 3D segmentation stage, we identify planar regions in the scan and compute the normal for each planar segment. We can use this information to create front-facing views of each individual plane by rotating the plane to lay along the x-y plane and using a synthetic camera pointing down the z-axis. We identify edges of this view using the Canny Edge algorithm [27].

The second technique we use for registration matches texture patterns visible via the laser's reflectivity values. Time-of-flight LIDAR scanners use a laser beam to scan an area and measure the time it takes for the laser to leave the scanner, hit a surface, and reflect back to the scanner in order to determine the depth of the point hit. The power of the returned beam contains some information about the type of surface struck. If a surface absorbs a large portion of the laser, only a small percentage of the original laser beam will be returned and a lower reflectivity value will be stored and vice versa. The returned value is also influenced by a number of factors including angle of incidence, distance to target, and atmospheric conditions [28], but the overall trend of reflectivity values tells us something about the changing surface texture found in a scene [29]. By visualizing the range of these values, we can create images that catch very similar texture variations to those seen in normal photographs as shown in Figure 2.

We visualize our 2D photographs so that the same properties that are emphasized in the wireframe and reflectivity images are also in focus. 2D Canny edges match the 3D wireframe edges and gradient patterns in photographs match reflectivity image gradients. Figures 1 and 2 show how applying these techniques cause the 2D and 3D data to look much more similar than they do in their original forms. In 3D, we use the planar segmentation information to focus on rocky areas in the scan. To focus on similar areas in the 2D data we identify line segments in the 2D images using the Line Segment Detector method [30]. Only features that are close to these line segments are used in the matching stage.

To actually match keypoints, we extract SIFT (Scale-Invariant Feature Transform) [31] features on both types of imagery and compare HOG (Histogram of Gradients) of the surrounding neighborhoods. This allows us to find areas that have either similar arrangements of edges in the wireframe and 2D edges image or similar gradient patterns in the reflectivity images and photographs. To ensure that corresponding keypoints are described with patches containing the same content and based in the same coordinate system, we extract patches at multiple scales surrounding each corner and orient them so that the dominant gradient direction of the patch points down the x-axis [32]. These keypoint matches are then used to estimate the camera projection matrix relating the photograph to the 3D scan using the six-point algorithm with Direct Linear Transform [33] and RANSAC.

IV. Experiments

We selected a vertical rock cut along the outer road adjacent to Highway 144 in Rolla, Missouri as our study site. There are two main areas we focus on in our evaluation. The first set of tests explores the design choice and accuracy of our 2D-3D registration pipeline. A high degree of accuracy is necessary for our registration pipeline to be of use for geological engineers to take digital measurements. The goal of our second group of tests is to see if rock measurements obtained by a trained engineer using traditional techniques are equivalent to the measurements obtained with our method, demonstrating the usefulness of our program.

For our 2D-3D registration evaluation, we broke down each test by looking at how well we were able to match the synthetic wireframe images to the Canny edge version of the photographs and the laser reflectivity images to the gradient version of the photographs. To show the benefit of using both types of data, we also looked at the accuracy of using matches from both types of image pairs combined.

For all of our 2D tests, we manually obtained a ground truth homography relating each image pair. We used this matrix to measure the repeatability of extracted 2D features and the accuracy of our 2D matches. For the 3D tests, we have a set of photographs obtained by the LIDAR

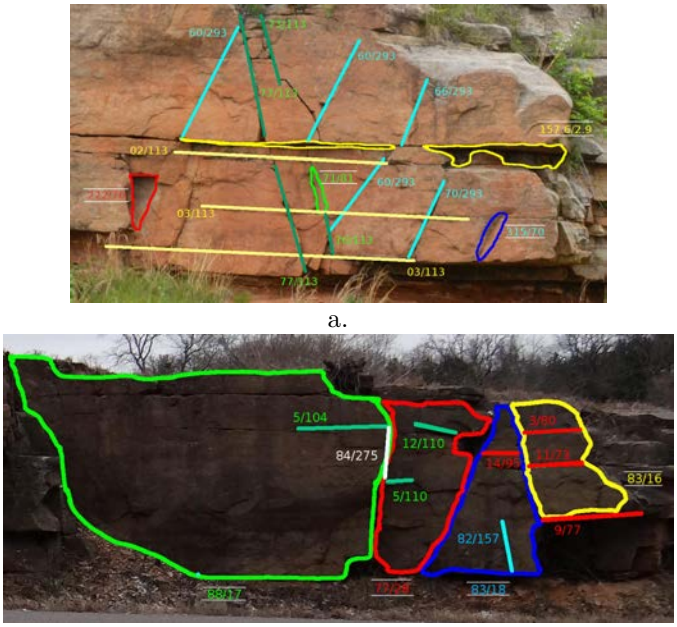

Fig. 4. Vertical rock cuts with manual measurements from Scan 1 (*a.*) and Scan 2 (*b.*) in Rolla showing traces (aqua, dark green, yellow, white, red lines) and facets (blue, light green, red and yellow outlines). Trace measurements are displayed in the format of "plunge/trend" and facet measurements are in the format "dip direction/dip angle".

TABLE III
PLUNGE AND TREND (TRACES) - MANUAL MEASUREMENTS VS. LIDAR VIEWER MEASUREMENTS *Scan 1 (S1) and Scan 2 S2)*

Line Color	Manual Plunge	Manual Trend	Software Plunge	Software Trend
S1 - Blue	70	293	65	273
S1 - Blue	66	293	70	273
S1 - Blue	60	293	51	273
S1 - Blue	60	293	61	285
S1 - Blue	60	293	59	275
S1 - Green	77	113	73	126
S1 - Green	78	113	76	121
S1 - Green	77	113	74	137
S1 - Green	76	113	75	123
S1 - Yellow	2	113	1	117
S1 - Yellow	3	113	1	102
S1 - Yellow	3	113	1	110
S2 - Red	9	77	10.4	82.7
S2 - Red	11	73	14.5	73.2
S2 - Red	3	80	1.6	85.2
S2 - Red	14	95	15.0	95.2
S2 - Blue	82	157	78.2	159.8
S2 - Green	5	110	5.3	105.1
S2 - Green	12	110	9.5	106.0
S2 - Green	5	104	4.4	104.3
S2 - White	84	275	82.2	264.8

TABLE IV
DIP AND DIP DIRECTION (FACETS) - MANUAL MEASUREMENTS VS. LIDAR VIEWER MEASUREMENTS *Scan 1 (S1) and Scan 2 S2)*

Plane Color	Manual Dip Direction	Manual Dip	Software Dip Direction	Software Dip
S1 - Blue	315	70	337	74
S1 - Green	71	81	101	76
S1 - Yellow	157.6	2.9	160	3.2
S1 - Red	222	70	235	81.2
S2 - Yellow	83	16	86.1	19.3
S2 - Blue	83	18	81.2	23.2
S2 - Red	77	28	86.0	27.0
S2 - Green	88	17	86.3	18.3

scanner used to collect Scan 1. The camera position in relation to the 3D point cloud is known for each of these photographs from data provided by the scanner. We matched the photographs from the scanner to the 3D data using both our pipeline and this ground truth information and compared the results.

The first test on our 2D-3D registration pipeline looks at our design choice of extracting SIFT features from our synthetic images and processed photographs for matching. We also considered using Harris Corners and Pseudo Corners [32], two other feature detectors that are generally well suited to images containing prominent lines. We measured how repeatable different types of features are between the image pairs being matched. Repeatability scores quantify what percentage of features extracted in one image have corresponding features extracted from a second image. As shown in Table I, SIFT features are more repeatable across our entire dataset.

After the 2D-2D matching stage of our pipeline, we also evaluated the accuracy of our keypoint matches based on HOG descriptions using our ground truth homographies. In Table II, we report the average number of matches obtained, the average number of inliers, the average match precision, and the average symmetrical transfer error of the matches [34]. We broke down these tests by reporting match results for just the wireframe to edge images, just the reflectivity to gradient images, and all of the matches combined. We can see that we tend to obtain a high percentage of correct matches with very low errors.

Finally, to show the error of our 2D-3D registration, we registered the photographs of Scan 1 with the 3D point cloud using only the matches obtained with the wireframe images, only the matches obtained with the reflectivity images, and using the two sets together. Using just the wireframe images, just the reflectivity, and both combined we have average errors of 0.6611 cm, 1.1142 cm, and 0.6496 cm respectively. Visual results of our 2D-3D registration are shown in Figure 3.

A geological engineer took manual measurements using a Brunton compass of various facets and traces on the rock cuts corresponding to the features that are highlighted in Figure 4. We selected the same lines and planes on 2D images using our software and compared them to the manually collected values. The actual measurements produced by our software were taken on the areas of the 3D scans corresponding to the selected areas on the photographs. Sets of plunge and trend measurements obtained manually and by our program are shown in Table III and a comparison of dip and dip direction results is shown in Table IV. We can see from these charts that the software and geological engineer's measurements of both facets and traces is consistent. The average difference between the measurements manually obtained by engineers and those produced with our program is 3.65 degrees.

V. CONCLUSION

Being able to measure discontinuities amongst rock faces is a necessary task for geological engineers to predict and handle potential rock failures. However, traditional approaches for obtaining these measurements can suffer from

sampling biases and be hazardous for engineers as they traverse hard-to-access and unstable rock faces. In this letter, we have proposed a method for using photographs and LIDAR scans to acquire these same measurements in a safer and more uniform capacity. We have focused on the fusion of these two data sources since photographs are simple to interact with and provide high resolution visual cues and LIDAR scans contain highly accurate 3D structural information. Registering these data sources is a difficult task since they are inherently different visually and numerically. To overcome these obstacles, we have presented a method for visualizing the common features of both data sources so that similar features can be extracted from both dimensions and matched. Our experimental results have shown that we can both accurately align 2D and 3D data and use this fusion to provide measurements very similar to those manually collected by engineers.

References

[1] M. Lato, J. Hutchinson, M. Diederichs, D. Ball, and R. Harrap, "Engineering monitoring of rockfall hazards along transportation corridors: using mobile terrestrial lidar," *Natural Hazards and Earth System Sciences*, vol. 9, no. 3, pp. 935–946, 2009.

[2] J. Kemeny and R. Post, "Estimating three-dimensional rock discontinuity orientation from digital images of fracture traces," *Computers & Geosciences*, vol. 29, no. 1, pp. 65–77, 2003.

[3] M. J. Lato and M. Vöge, "Automated mapping of rock discontinuities in 3d lidar and photogrammetry models," *International Journal of Rock Mechanics and Mining Sciences*, vol. 54, pp. 150–158, 2012.

[4] A. Strouth and E. Eberhardt, "The use of lidar to overcome rock slope hazard data collection challenges at afternoon creek, washington," in *Methods for Rock Face Characterization Workshop US Symposium on Rock Mechanics*. Golden, CO: American Rock Mechanics Association, June 17-21 2006, pp. 49–62.

[5] M. J. Lato, M. S. Diederichs, and D. J. Hutchinson, "Bias correction for view-limited lidar scanning of rock outcrops for structural characterization," *Rock mechanics and rock engineering*, vol. 43, no. 5, pp. 615–628, 2010.

[6] M. I. Olariu, J. F. Ferguson, C. L. V. Aiken, and X. Xu, "Outcrop fracture characterization using terrestrial laser scanners: Deep-water jackfork sandstone at big rock quarry, arkansas," *Geosphere*, vol. 4, no. 1, pp. 247–259, 2008.

[7] J. N. Otoo, N. H. Maerz, L. Xiaoling, and Y. Duan, "3-d discontinuity orientations using combined optical imaging and lidar techniques," in *Proceedings of the 45th US rock mechanics symposium*, 2011.

[8] K. Khoshelham, D. Altundag, D. Ngan-Tillard, and M. Menenti, "Influence of range measurement noise on roughness characterization of rock surfaces using terrestrial laser scanning," *International Journal of Rock Mechanics and Mining Sciences*, vol. 48, no. 8, pp. 1215–1223, 2011.

[9] R. Post, "Characterizing of joints and fractures in a rock mass using digital image processing," Ph.D. dissertation, MS Thesis, University of Arizona, Tucson, AZ 105 pp, 2001.

[10] W. C. Haneberg, "Book and software reviews sirovision," *Environmental & Engineering Geoscience*, vol. 12, no. 3, pp. 283–285, 2006.

[11] W. Hanberg, "Using close range terrestrial digital photogrammetry for 3-d rock slope modeling and discontinuity mapping in the united states," in *Bulletin of Engineering Geology and the Environment*, vol. 67, no. 4, 2008, pp. 457–469.

[12] J. L. Schönberger and J. Frahm, "Structure-from-motion revisited," in *Computer Vision and Pattern Recognition*. IEEE, 2016.

[13] M. Sturzenegger and D. Stead, "Close-range terrestrial digital photogrammetry and terrestrial laser scanning for discontinuity characterization on rock cuts," *Engineering Geology*, vol. 106, no. 3, pp. 163–182, 2009.

[14] G. Gigli and N. Casagli, "Semi-automatic extraction of rock mass structural data from high resolution lidar point clouds," *International Journal of Rock Mechanics and Mining Sciences*, vol. 48, no. 2, pp. 187–198, 2011.

[15] D. García-Sellés, O. Falivene, P. Arbués, O. Gratacos, S. Tavani, and J. A. Muñoz, "Supervised identification and reconstruction of near-planar geological surfaces from terrestrial laser scanning," *Computers & Geosciences*, vol. 37, no. 10, pp. 1584–1594, 2011.

[16] A. Riquelme, A. Abellán, R. Tomás, and M. Jaboyedoff, "A new approach for semi-automatic rock mass joints recognition from 3d point clouds," in *Computers and Geosciences*, vol. 68, 2014, pp. 38–52.

[17] J. N. Otoo, N. H. Maerz, X. Li, and Y. Duan, "Verification of a 3-d lidar viewer for discontinuity orientations," *Rock mechanics and rock engineering*, vol. 46, no. 3, pp. 543–554, 2013.

[18] R. Schnabel, R. Wahl, and R. Klein, "Efficient ransac for point-cloud shape detection," in *Computer graphics forum*, vol. 26, no. 2. Wiley Online Library, 2007, pp. 214–226.

[19] N. Brodu and D. Lague, "3d terrestrial lidar data classification of complex natural scenes using a multi-scale dimensionality criterion: Applications in geomorphology," *ISPRS Journal of Photogrammetry and Remote Sensing*, vol. 68, pp. 121–134, 2012.

[20] Y. Li, Q. Zheng, A. Sharf, D. Cohen-Or, B. Chen, and N. Mitra, "2D-3D fusion for layer decomposition of urban facades," in *International Conference on Computer Vision*. IEEE, 2011, pp. 882–889.

[21] I. Stamos, L. Liu, C. Chen, G. Wolberg, G. Yu, and S. Zokai, "Integrating automated range registration with multiview geometry for the photorealistic modeling of large-scale scenes," *International Journal of Computer Vision*, vol. 78, no. 2, pp. 237–260, 2008.

[22] G. Pandey, J. R. McBride, S. Savarese, and R. M. Eustice, "Automatic targetless extrinsic calibration of a 3d lidar and camera by maximizing mutual information," *Proc. AAAI National Conference on Artifical Intelligence*, 2012.

[23] B. C. Matei, N. V. Valk, Z. Zhu, and H. Cheng, "Image to lidar matching for geotagging in urban environments," in *Applications of Computer Vision*. IEEE, 2013, pp. 413–420.

[24] L. Yu, K. Efstathiou, P. Isenberg, and T. Isenberg, "Cast: Effective and efficient user interaction for context-aware selection in 3d particle clouds," vol. 22, no. 1. IEEE, 2016, pp. 886–895.

[25] F. Bacim, M. Nabiyouni, and D. A. Bowman, "Slice-n-swipe: A free-hand gesture user interface for 3d point cloud annotation," in *Symposium on 3D User Interfaces*. IEEE, 2014, pp. 185–186.

[26] A. Irschara, C. Zach, J. Frahm, and H. Bischof, "From structure-from-motion point clouds to fast location recognition," in *Computer Vision and Pattern Recognition, 2009. CVPR 2009. IEEE Conference on*. IEEE, 2009, pp. 2599–2606.

[27] J. Canny, "A computational approach to edge detection," *Pattern Analysis and Machine Intelligence*, no. 6, pp. 679–698, 1986.

[28] G. Petrie and C. Toth, *Topographic Laser Ranging and Scanning*. CRC Press, 2008.

[29] D. Carrea, A. Abellan, F. Humair, B. Matasci, M. Derron, and M. Jaboyedoff, "Correction of terrestrial lidar intensity channel using oren nayar reflectance model: An application to lithological differentiation," *ISPRS Journal of Photogrammetry and Remote Sensing*, vol. 113, pp. 17–29, 2016.

[30] R. G. V. Gioi, J. Jakubowicz, J. M. Morel, and G. Randall, "Lsd: A fast line segment detector with a false detection control," *Pattern Analysis and Machine Intelligence*, vol. 32, no. 4, pp. 722–732, 2010.

[31] D. G. Lowe, "Distinctive image features from scale-invariant keypoints," *International Journal of Computer Vision*, vol. 60, no. 2, pp. 91–110, 2004.

[32] B. Morago, G. Bui, and Y. Duan, "An ensemble approach to image matching using contextual features," *IEEE Trans. on Image Processing*, 2015.

[33] R. Hartley and A. Zisserman, *Multiple View Geometry*. Cambridge, United Kingdom: Cambridge University Press, 2010.

[34] N. Snavely, S. Seitz, and R. Szeliski, "Modeling the world from internet photo collections," *International Journal of Computer Vision*, vol. 80, no. 2, pp. 189–210, 2007.